Remote Sensing of Environment 212 (2018) 260–272

Contents lists available at ScienceDirect

Remote Sensing of Environment

journal homepage: www.elsevier.com/locate/rse

A fuel moisture content and flammability monitoring methodology for continental Australia based on optical remote sensing

Marta Yebra[a,b,*], Xingwen Quan[c], David Riaño[d,e], Pablo Rozas Larraondo[f], Albert I.J.M. van Dijk[a,b], Geoffrey J. Cary[a,b]

[a] Fenner School of Environment and Society, The Australian National University, Acton, ACT, Australia
[b] Bushfire and Natural Hazards Cooperative Research Centre, Melbourne, Australia
[c] School of Resources and Environment, University of Electronic Science and Technology of China, Chengdu, Sichuan, China
[d] Center for Spatial Technologies and Remote Sensing (CSTARS), University of California, 139 Veihmeyer Hall, One Shields Avenue, Davis, CA 95616, USA
[e] Instituto de Economía, Geografía y Demografía (IEGD), Centro de Ciencias Humanas y Sociales (CCHS), Consejo Superior de Investigaciones Científicas (CSIC), Albasanz 26-28, 28037 Madrid, Spain
[f] National Computational Infrastructure, The Australian National University, Acton, ACT, Australia

ARTICLE INFO

Keywords:
Fire occurrence
Fire risk
PROSAIL inversion
GEOPROSAIL inversion
MODIS
Grasslands
Shrubs
Forests

ABSTRACT

Fuel Moisture Content (FMC) is one of the primary drivers affecting fuel flammability that lead to fires. Satellite observations well-grounded with field data over the highly climatologically and ecologically diverse Australian region served to estimate FMC and flammability for the first time at a continental-scale. The methodology includes a physically-based retrieval model to estimate FMC from MODIS (Moderate Resolution Imaging Spectrometer) reflectance data using radiative transfer model inversion. The algorithm was evaluated using 360 observations at 32 locations around Australia with mean accuracy for the studied land cover classes (grassland, shrubland, and forest) close to those obtained elsewhere (r^2 = 0.58, RMSE = 40%) but without site-specific calibration. Logistic regression models were developed to generate a flammability index, trained on fire events mapped in the MODIS burned area product and four predictor variables calculated from the FMC estimates. The selected predictor variables were actual FMC corresponding to the 8-day and 16-day period before burning; the same but expressed as an anomaly from the long-term mean for that date; and the FMC change between the two successive 8-day periods before burning. Separate logistic regression models were developed for grassland, shrubland and forest. The models obtained an "Area Under the Curve" calculated from the Receiver Operating Characteristic plot method of 0.70, 0.78 and 0.71, respectively, indicating reasonable skill in fire risk prediction.

1. Introduction

The Fuel Moisture Content (FMC) of live bushfire fuel affects fire danger and fire behaviour, as it strongly influences the key components of flammability including ignitability, fire sustainability and combustibility (Anderson, 1970). 'Mega-fires' – extreme fire events with dramatic impacts on people and environment – generally occur after periods of moderate to severe drought (Stephens et al., 2014) in part due to drought effects on FMC. Therefore, spatially comprehensive and temporally frequent estimates of FMC should be a fundamental component of fire danger rating systems in support of a wide range of fire risk management and response activities, such as prescribed burning and pre-positioning firefighting resources.

In recent years, there has been considerable development in the estimation of FMC from satellite imagery. The literature is dominated by studies that apply either statistical (empirical) or physical model-based methods to coarse resolution data covering the visible, near infrared, and shortwave infrared regions of the electromagnetic spectrum (Yebra et al., 2013). Empirical relationships have the drawback of being sample-specific, but on the other hand, the selection and parameterization of physically-based algorithms is challenging. Previous studies mainly retrieved FMC in Mediterranean and Temperate ecosystems in Europe (Al-Moustafa et al., 2012; García et al., 2008; Jurdao et al., 2013b; Yebra and Chuvieco, 2009b), Western North America (Casas et al., 2014; Hao and Qu, 2007; Peterson et al., 2008) and southeastern Australia (Caccamo et al., 2012; Nolan et al., 2016). Further research is needed to assess the full utility of FMC estimation across other fire-prone ecosystems (Yebra et al., 2013).

The conversion of FMC values into a Flammability Index (FI) can be an important additional step that facilitates the inclusion of FMC

* Corresponding author at: Fenner School of Environment and Society, The Australian National University, Acton, ACT, Australia.
E-mail address: marta.yebra@anu.edu.au (M. Yebra).

https://doi.org/10.1016/j.rse.2018.04.053
Received 20 November 2017; Received in revised form 30 April 2018; Accepted 30 April 2018

estimates into an integrated fire risk assessment system (Chuvieco et al., 2014). Research has produced several methods for this conversion based on (i) the concept of moisture of extinction, defined as the moisture threshold above which fire cannot be sustained (Chuvieco et al., 2004a); (ii) critical FMC thresholds derived from empirical statistical relations between FMC and fire occurrence (Dennison and Moritz, 2009; Nolan et al., 2016); and (iii) fitting a continuous logistic probability model between fire occurrence and FMC (Chuvieco et al., 2009a; Jurdao et al., 2012). However, so far none of these methods have been evaluated across a region as climatologically and ecologically diverse as Australia.

Through the use of remotely sensed data, this paper aims to derive the first continental-wide FMC and flammability monitoring methodology for Australia. The overarching objective is to contribute to the development of operational tools that can assist in better resources allocation in fire protection and response and improved awareness of fire risk to life and property.

2. Data

2.1. Live fuel moisture content measurements

Existing field FMC data had been collected at 32 sites across Australia as part of fuel remote sensing studies (Table 1, Fig. 1). All sites were selected to be sufficiently homogeneous to assume that the field measurements would be representative within a 2 × 2 MODIS 500 m pixels window. The data was collected between 2004 and 2014 by different research groups, during various time periods, and for different land cover classes, including grassland and crop (Newnham et al., 2011), shrubland (Caccamo et al., 2012) and forest (Caccamo et al., 2012; Nolan et al., 2016). These resulted in 3 to 37 observations over time per site (Table 1). Two of the heathland sites of Caccamo et al. (2012) were not considered here due to incomplete FMC data (their DNR site), and because of a geocoding anomaly (their LPF site). BCA2 location was also anomalous in Table 1 of Caccamo et al. (2012) but a revised longitude was provided by the authors (Table 1). Of the 25 grassland sites reported by Newnham et al. (2011), ten were not considered: four had no live FMC measurements, another four were represented by only one measurement, another one contained a geocoding anomaly and another one had unrealistically low values.

As part of this study, new FMC data were collected at one grassland and two forest sites in the Australian Capital Territory. Sample sites included a grassland site adjacent to Coppins Crossing Road and two forest sites in Namadgi National Park (Table 1).

At the grassland site, ten grass samples of about 80 g each were collected on 33 occasions between 17 November 2014 and 20 April 2016, along a 670 m transect where in-situ NDVI sensors were installed. Each sample was a mixture of live and dead but always standing material, and therefore FMC values lower than 30% were observed over some days during the summer periods. At each forest site, four samples were collected from each of three forest layers (canopy, elevated fuel and near-surface fuel) on 19–21 occasions between 19 October 2015 and 19 April 2016. Leaves from the canopy were collected using an arborist throw-line launcher following Youngentob et al. (2016). The collected samples were placed in a sealed bag and returned to the laboratory to weigh (m_f) and transferred into paper bags to be oven dried for 24 h at 105 °C (Matthews, 2010). Once dried, the samples were weighed again to determine dry weight (m_d). The FMC of each sample was calculated as the percentage difference of fresh and dry weight (Eq. 1).

Table 1
Description of the field sites used in this study. NSW: New South Wales, ACT: Australian Capital Territory TAS: Tasmania, WA: Western Australia, VIC: Victoria, NP: National Park. $\overline{FMC}$, FMC_{std} and n are the mean, standard deviation and number of observations of the field FMC at each site (after spikes were removed). CV_{Sept} and CV_{Jan} are the NDVI coefficient of variation for September 2015 (spring) and January 2016 (summer) for a 40 × 40 Landsat-8 pixels window. *Indicate sites used for the calibration of Nolan et al. (2016)'s empirical model. Caccamo et al. (2012) used a 70% and 30% random sample for calibration and validation respectively.

ID	Name	Region	Fuel class	Latitude	Longitude	$\overline{FMC}$	FMC_{std}	CV_{Sept}	CV_{Jan}	n	Source
1	Majura	ACT	Grassland	−35.2778	149.1966	68	45	0.2	0.1	37	Newnham et al. (2011)
2	Tidbinbilla	ACT	Grassland	−35.4191	148.9506	95	64	0.1	0.1	33	Newnham et al. (2011)
3	Coppins crossing road	ACT	Grassland	−35.2787	149.0559	115	83	0.1	0.2	33	This study
4	Ballan	VIC	Grassland	−37.6352	144.2213	163	71	0	0.1	4	Newnham et al. (2011)
5	Caldermeade_Park	VIC	Grassland	−38.2257	145.5633	60	19	0.2	0.2	5	Newnham et al. (2011)
6	Kaduna_Park	VIC	Grassland	−38.0895	145.4307	93	23	0.2	0.2	5	Newnham et al. (2011)
7	Murrayville grassland	VIC	Grassland	−35.2414	141.2247	64	60	0.1	0.3	7	Newnham et al. (2011)
8	Murrayville wheat	VIC	Crop-non irrigated	−35.2405	141.2152	114	56	0.1	0.1	7	Newnham et al. (2011)
9	Parry lagoons	WA	Grassland	−15.5866	128.2338	65	27	0.1	0.1	12	Newnham et al. (2011)
10	Silent grove sandstone	WA	Grassland	−17.1309	125.3739	43	21	0.2	0.1	9	Newnham et al. (2011)
11	Silent grove black soil	WA	Grassland	−17.0629	125.2609	52	28	0.2	0.1	4	Newnham et al. (2011)
12	Mount hart sandstone	WA	Grassland	−17.0297	125.1159	55	30	0.1	0.2	9	Newnham et al. (2011)
13	Simcocks	WA	Grassland	−34.2170	116.3831	87	62	0.1	0.1	5	Newnham et al. (2011)
14	Lorna glen	WA	Grassland	−26.1629	121.5588	43	11	0.1	0.1	10	Newnham et al. (2011)
15	RNP	NSW	Shrubland	−34.1333	151.0667	102	12	0	0	15	Caccamo et al. (2012)
16	RNP2	NSW	Shrubland	−34.1667	151.0333	100	10	0.1	0.1	13	Caccamo et al. (2012)
17	RNP3	NSW	Shrubland	−34.1333	151.100	100	10	0.1	0.1	15	Caccamo et al. (2012)
18	TNP	NSW	Forest	−34.2167	150.5333	102	8	0.1	0.1	12	Caccamo et al. (2012)
19	BCA	NSW	Forest	−34.3167	150.4667	98	7	0	0.1	12	Caccamo et al. (2012)
20	BCA2	NSW	Forest	−34.2667	150.5000	98	6	0.1	0.1	11	Caccamo et al. (2012)
21	Cumberland plain woodland*	NSW	Forest	−33.6153	150.7237	106	34	0	0	19	Nolan et al. (2016)
22	Tumbarumba forest*	NSW	Forest	−35.6566	148.1517	156	20	0.1	0.1	8	Nolan et al. (2016)
24	Megalong	NSW	Forest	−33.6895	150.2342	102	7	0.1	0.1	5	Nolan et al. (2016)
25	Blue mountain NP (Ridge)	NSW	Forest	−33.6602	150.6177	107	1	0.1	0	4	Nolan et al. (2016)
26	Blue mountain NP (Gully)	NSW	Forest	−33.6578	150.6161	114	7	0.1	0.1	4	Nolan et al. (2016)
27	Blue mountains NP (open woodland)	NSW	Forest	−33.6107	150.6384	100	11	0.1	0.1	5	Nolan et al. (2016)
28	Blue mountains NP (denser canopy)	NSW	Forest	−33.7447	150.3900	108	12	0.1	0	4	Nolan et al. (2016)
31	Bago state forest	NSW	Forest	−35.6468	148.1483	164	27	0.2	0.2	3	Nolan et al. (2016)
30	Wombat forest*	VIC	Forest	−37.4215	144.0938	101	20	0.1	0.1	10	Nolan et al. (2016)
23	Tamboon state forest	VIC	Forest	−37.5679	149.1088	114	8	0.1	0.1	3	Nolan et al. (2016)
29	Namadgi National Park 1	ACT	Forest	−35.5979	148.8165	130	16	0.1	0.1	19	This study
32	Namadgi National Park 2	ACT	Forest	−35.6071	148.8657	137	11	0.2	0.1	18	This study

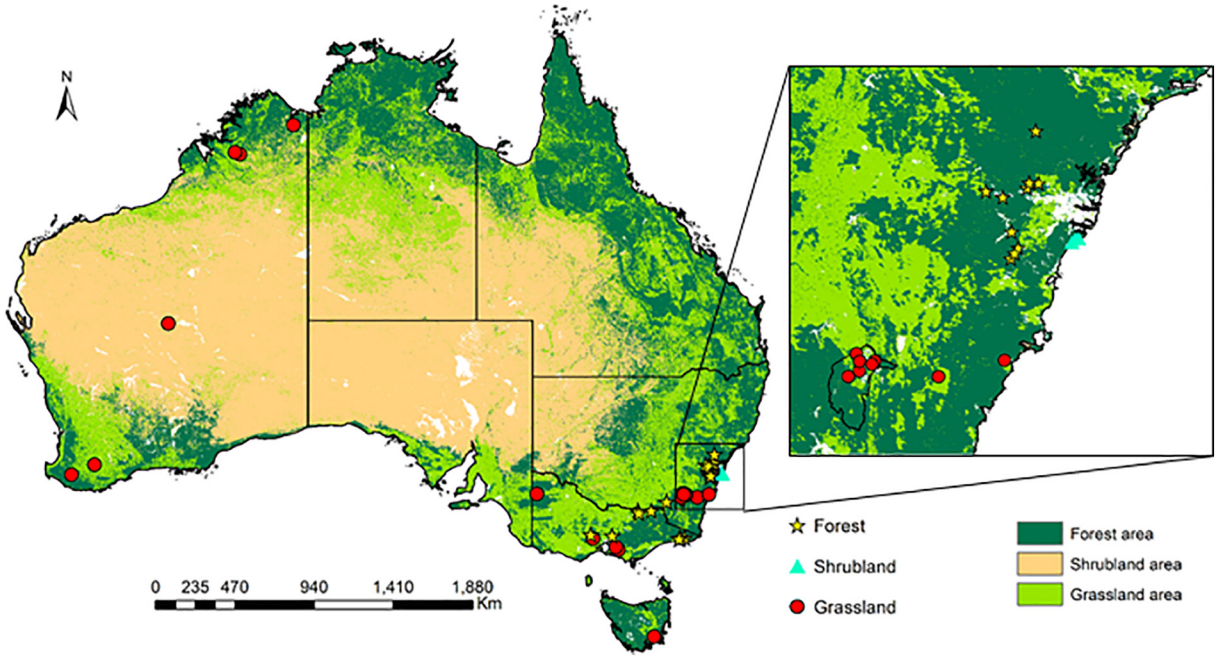

Fig. 1. Location of the validation sites.

$$FMC = \frac{m_f - m_d}{m_d} \times 100\% \quad (1)$$

Time series of field-measured FMC at some sites contained 'spikes' and sharp drops that could not represent any realistic biophysical change. These anomalous measurements could be due to sampling after rain or dew events. Two other feasible explanations are that plant parts other than leaves (e.g., fruits, flowers, galls or twigs) could have been included in samples, or that the different proportion of juvenile and adults eucalyptus leaves sampled to make up a representative sample. Spikes can impact the evaluation of the model estimates and therefore were removed before further analysis using a 3-day window and the standard deviation as proposed by Lymburner et al. (2011):

$$\frac{|FMC_i - \mu|}{\sigma} > x \quad (2)$$

where FMC_i is the time series value, μ is the median of three successive measures, σ is the standard deviation across the time series and x is the critical value. Lymburner et al. (2011) applied x = 2.1 but here a more restrictive value x = 1 avoided unrealistically abrupt changes in FMC within consecutive sampling dates. This approach filtered out 15 out of the 375 observations.

2.2. Satellite data

We used MODIS (Moderate Resolution Imaging Spectrometer) Collection 5 products hosted at the National Computing Infrastructure in Canberra, Australia (www.nci.org.au). The original data were supplied by the Land Processes Distributed Active Archive Center (LPDAAC) at the U.S. Geological Survey (USGS) Earth Resources Observation and Science Center (EROS) (http://lpdaac.usgs.gov).

2.2.1. Reflectance

The MODIS reflectance product MCD43A4 Collection 5 (DOI: https://doi.org/10.4225/41/5837cd92ada9f) (Strahler et al., 1999) was selected as the source of surface reflectance following Jurdao et al. (2013b). MCD43A4 provides 500-metre reflectance data adjusted using a bidirectional reflectance distribution function (BRDF) to estimate the reflectance values as if they were observed at nadir. The quality information of the MCD43A4 pixel reflectance is stored in the MODIS BRDF/Albedo Quality Collection 5 product (MCD43A2, DOI: https://doi.org/10.4225/41/5837cd2c8fa99). This product was used to remove pixels with partial or complete cloud cover or low data quality. We only considered 'good quality' full BRDF data indicated by a zero value in the "BRDF_Albedo_Band_Quality" layer.

To allow for locational inaccuracies in mapping field sampling locations to MODIS pixels, the algorithm extracted the median of the closest 2 × 2 MODIS pixels to each field sampling location. A 40 × 40 Landsat-8 pixels window served to calculate the NDVI coefficient of variation (CV) for September 2015 (spring) and January 2016 (summer) and hence provide evidence of the field sites homogeneity within the 2 × 2 MODIS 500 m pixels window (Table 1). Clouds and cloud-shadow were masked and images with < 80% good pixels dropped. MCD43A4 and MCD43A2 Collection 5 are calculated every 8-days based on 16 days of MODIS Terra and Aqua observations. Therefore, field sampling dates were assigned the MODIS composite that contained the observations of the 8 days in the middle. For example, field sampling between ordinal day (OD) 5–12 (i.e., 5–12 January) corresponds to the MODIS composite starting at OD 1, which is constructed from data collected between OD 1 and 16. Similarly, sampling between OD 13–20 corresponds to the composite starting on OD 9, and so on.

2.2.2. Land cover type

The MODIS land cover product MCD12Q1 Collection 5 (Friedl et al., 2010) (DOI: https://doi.org/10.4225/41/5837cf4813ffd) was used to classify vegetation type. From the four global land cover classification systems included in MCD12Q1, we selected the IGBP classification scheme (Loveland and Belward, 1997). Since MCD12Q1 is only available from 2001 to 2013, we continued used the year 2013 for the years 2014 to 2016. The vegetation categories included in the IGBP classification scheme were re-classified into the three land cover classes considered here: grassland, shrubland, and forest. Specifically, the IGBP classes grasslands and croplands where combined into the class grasslands; closed and open shrublands into shrublands; and the forest classes (evergreen needleleaf forest, evergreen broadleaf forest, deciduous needleleaf forest, deciduous broadleaf forest, woody savannas and savannas) into forest. Classes that did not fit in any of the above three types (water, permanent wetlands, urban and built-up, cropland/

natural vegetation mosaic, snow and ice and barren or sparsely vegetated) were not assessed.

2.2.3. Burned area

The MODIS Burned Area (BA) product MCD64A1 Collection 5 (Giglio et al., 2009) (DOI: https://doi.org/10.4225/41/5837cbc90d2b9) was selected as a measure of fire occurrence. The product is generated every month at 500 m spatial resolution and was found to be the most accurate large-scale BA product currently available in a comparative study by Padilla et al. (2015). MCD64A1 is based on MODIS spectral indices, a measure of temporal pattern and active fire observations. For each grid cell, the data contains (*i*) the ordinal day-of-burn, (*ii*) the uncertainty in the day-of-burn, (*iii*) a quality assurance index, and the (*iv*) first and (*v*) last day of reliable change detection. Information on the ordinal day-of-burn and the uncertainty in day-of-burn was used to determine the locations and dates for all fires in Australia from 2001 to 2015.

3. Methods

3.1. Fuel moisture content retrieval

The methodology to derive FMC is illustrated in Fig. 2. We applied three reference Look-Up Tables (LUTs) generated in previous studies for grasslands [$LUT_{Grassland}$; (Jurdao et al., 2013a; Yebra et al., 2008)], shrublands [$LUT_{Shrubland}$;(Jurdao et al., 2013a; Yebra and Chuvieco, 2009a)], and forest [LUT_{Forest}; (Jurdao et al., 2013b)]. These three land cover classes have different structural characteristic and biochemical composition. Their spectral signatures were simulated using different radiative transfer models (RTMs) listed in Table 2. PROSPECT 1 (Jacquemoud and Baret, 1990) was coupled with SAILH 1 (Kuusk, 1991; Verhoef, 1984) to simulate the grassland and shrubland spectra, and coupled with GeoSail (Huemmrich, 2001) to simulate the forest spectra. PROSPECT is a leaf-level RTM that describes a leaf as a stack of plates with absorbing and diffusing constituents, and is commonly used to calculate reflectance and transmittance of broadleaves from 400 nm to 2500 nm. The calculated reflectance and transmittance are expressed as a function of several scattering and absorption components: a leaf structure parameter (N, unit-less), leaf chlorophyll content (C_{ab}, $\mu g\,cm^{-2}$), Dry Matter Content (DMC, $g\,cm^{-2}$), Equivalent Water Thickness (EWT, $g\,cm^{-2}$), leaf brown pigment (C_{bp}, unit-less) and carotenoid content (C_{ar}, $\mu g\,cm^{-2}$). The SAILH model is a 1D turbid medium RTM specifically designed for homogeneous plant canopies using the following input parameters: leaf-level hemispheric reflectance (nm); and leaf transmittance (nm) for each waveband (here taken from), two leaf inclination distribution function parameters, ($LIDF_a$ and $LIDF_b$; unit-less); soil factor (psoil, unit less); Leaf Area Index (LAI, unit less); hot spot factor (hspot, unit less); the Sun zenith angle (tts, °); observer zenith angle (tto. °) and relative azimuth angle (psi, °). The GeoSail model combines the SAIL turbid medium model (same as SAILH but without considering the hotspot parameter) that simulates the reflectance and transmittance of the tree crowns with a geometric model that calculates the amount of shadowed and illuminated components in a scene. The GeoSail model requires the following input parameters: leaf-level spectral reflectance and transmission for each waveband (here taken from PROSPECT); LIDF; LAI; spectral reflectance of the background; tts; shape of the crowns (cylinder or cone); height to width ratio of the crown (CHW); and crown coverage (ccov).

Table 2
Radiative transfer models used for the generation of each LUT and the source reference to details on the parameterization of each model.

Land Cover class	RTM	Representative species	Reference
Grass	PROSAILH	*Leontodon longirostris*, *Poa bulbosa*, *Vulpia ganiculata*, *Echium plantaginerum*, *Avena barbata*, *Plantago coronopus*, *Rumex angiocarpus*	Yebra et al. (2008) Jurdao et al. (2013a)
Shrub	PROSAILH	*Cistus ladanifer*, *Rosmarinus officinalis*, *Erica australis*, *Phillyrea angustifolia*	Yebra and Chuvieco (2009b) Jurdao et al. (2013a)
Forest	PROGeoSail	*Quercus ilex*, *Quercus faginea*, *Pinus halepensis*, *Eucalyptus globulus*, *Fagus sylvatica*, *Quercus robur*	Jurdao et al. (2013b)

Detailed ecological information for the main vegetation types of Spain was used to parameterize the original RTMs. This information was obtained from the literature, laboratory experiments and field campaigns (Table 2). For example, Yebra et al. (2008) and Jurdao et al.

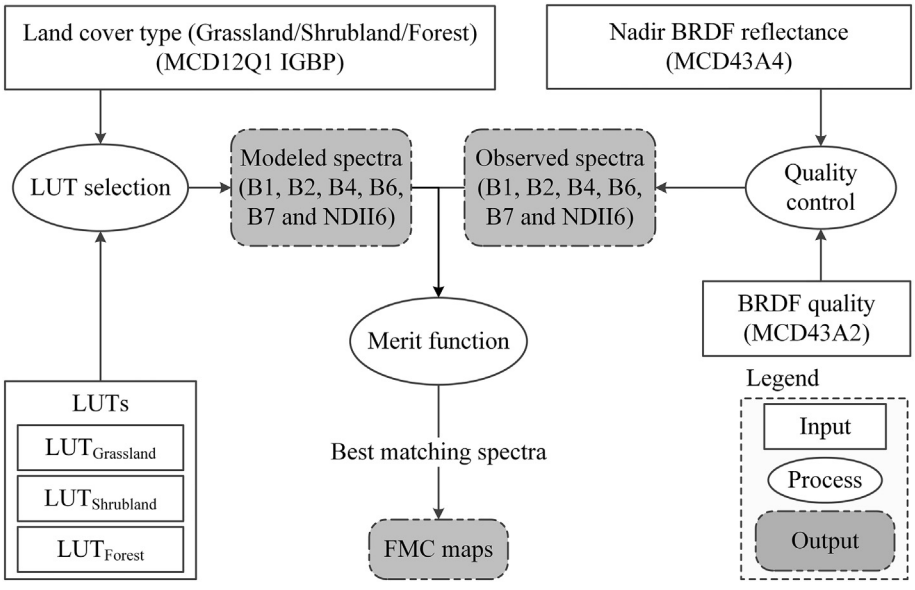

Fig. 2. Diagram illustrating the methodology to retrieve FMC.

(2013a) used linear relationships between field observations of grassland FMC and LAI to avoid unrealistic combinations of these parameters.

The provisional assumption made here was that the three LUTs developed for Spain can reasonably be used to retrieve FMC in Australia using MODIS reflectance data. Therefore, we derived FMC across Australia using information on land cover class to constrain the inversion. For every MCD43A4 grid cell of accepted quality, the MCD12Q1 land cover map (reclassified into grassland, shrubland and forest categories) was used to select the corresponding LUT. All simulated reflectance in the LUT were subsequently compared to the observed reflectance of the grid cell using a merit function. Out of the merit functions proposed in the literature (Yebra et al., 2013), the spectral angle (SA) was found most sensitive to changes in the reflectance from plant drying by Jurdao et al. (2014) and therefore was used here. The spectral angle is calculated as the arccosine of the product of the spectra (Kruse et al., 1993):

$$\mathrm{SA}(\mathrm{v},\mathrm{w}) = \cos^{-1}\left[\frac{\sum_{i=1}^{m} v_i w_i}{\sqrt{\sum_{i=1}^{m} v_i^2}\sqrt{\sum_{i=1}^{m} w_i^2}}\right] \quad (3)$$

where v and w are the satellite-observed and the LUT predicted reflectance, respectively, both considered as a m-dimensional vector, with $m = 6$ being the number of bands considered. MODIS bands 1 (red, 620–670 nm), 2 (near infrared, 841–876 nm), 4 (green, 545–565 nm), 6 (SWIR2, 1628–1652 nm) and 7 (SWIR3, 2105–2155 nm) were used. Band 3 (blue, 459–479 nm) was discarded because variation in FMC has no effect in blue wavelengths (Bowyer and Danson, 2004) whereas measurement errors are greater than in longer wavelengths (Roy et al., 2014 and references therein). Band 5 (SWIR1, 1230–1250 nm) was discarded because of the radiometric problems of the MODIS Terra data for this band. In addition to the mentioned MODIS bands, the Normalized Difference Infrared Index, (NDII6, Hardisky et al., 1983), here calculated as the normalized difference between MODIS bands 6 and 2, was also included in the vectors v and w. NDII is a vegetation index specifically designed to maximise sensitivity to vegetation water content and minimise sensitivity to other leaf and canopy variables, and its inclusion has been proven to improve the estimates of RTM model inversion (Chuvieco et al., 2009b).

The SA values for the simulated spectra from the LUT were ranked by their similarity to the observed MODIS spectrum. Rather than adopting only a single 'optimal' result, it was tested whether the estimates improved if instead the average of a larger ensemble of 'near-optimal' RTM results of variable size was calculated. The optimal ensemble size was selected as that presenting the lowest Root Mean Square Error (RMSE) and highest correlation coefficient between retrieved and field-measured FMC. This approach has the additional benefit of producing a distribution of similarly plausible FMC values, which was characterised by calculating the ensemble standard deviation as a measure of retrieval uncertainty.

The described algorithm was implemented in Python using GDAL to read the original MODIS files and Numpy (van der Walt et al., 2011) to perform the numerical processing.

3.2. Flammability index

The FMC retrievals were used to map a dimensionless Flammability Index (FI) based on logistic regression models between fire occurrence derived from the BA MCD64A1 product (the binary dependent variable) and predictor variables derived from the satellite FMC estimates described in the previous section. The training sample was constructed as a series of data pairs, in which each data pair includes (*i*) FMC of a pixel before burning, and (*ii*) the median FMC of a representative sample of unburned pixels that is sufficiently close to represent a similar land cover class, but did not burn. The median is preferred to the average in order to avoid the influence of outliers in the final FMC estimations. An underlying assumption is that the latter pixels did not burn because they had higher FMC, although many other explanations are of course possible (see discussion). Provided the paired burned and unburned pixels show a systematic difference in FMC, this approach can still produce useful results, and using a Mann Whitney *U* test, Jurdao et al. (2012) demonstrated this to be the case. The construction of the training data set described below is based on the Australian dataset using selected candidate variables for the model from Jurdao et al. (2012). An important feature of the pairing is that there are equal numbers of entries representing burned and unburned pixels, respectively, and hence the average FI (i.e., the probability of fire occurrence) in the training data is 0.5. The predicted FI should hence be interpreted as a dimensionless flammability index (ranging from 0 to 1) defined in the context of the training data, and not as a prediction of actual fire probability as the index does not account for the ignition source. Following Jurdao et al. (2012) we use a cumulative logistic distribution function to predict FI (Eqs. 4–5):

$$FI = \frac{1}{1 + e^{-z}} \quad (4)$$

$$z = a + \beta_1 x_1 + \beta_2 x_2 + \ldots + \beta_n x_n \quad (5)$$

where FI is the Flammability Index (equalling the probability of fire occurrence in the training sample), a is the model intercept, β_1, …,β_n are the equation coefficients, x_1, x_2, …,x_n are the independent variables.

Based on the analysis of Jurdao et al. (2012), four candidate variables were calculated from the FMC estimates: (*i*) $FMC_{t\text{-}1}$, or FMC corresponding to the 8-day period prior to the 8-day period including the fire date; (*ii*) $FMC_{t\text{-}2}$, or FMC values of the 8-day period prior to FMCt-1; (*iii*) FMC Difference (FMC_D); or FMC variation between the two periods ($FMC_{t\text{-}2}$ - $FMC_{t\text{-}1}$), representing a rate of change and (iv) FMC Anomaly (FMC_A), or the departure of $FMC_{t\text{-}1}$ from the average FMC value for that 8-day period ($\overline{FMC}$) over the time series (2001–2016), which emphasises atypically low or high FMC in relation to the historical record.

The non-parametric Mann-Whitney *U* test for large samples determined which predictor variables ($FMC_{t\text{-}1}$, $FMC_{t\text{-}2}$, FMC_D and FMC_A) showed the most significant difference between burned and unburned areas. Also, the dependence between the four variables was tested using the Pearson's correlation coefficient. A variable was discarded as an independent candidate if it was strongly correlated with already selected variables (Pearson coefficient > 0.7, $p < 0.05$).

To construct the flammability models, a burned pixel was selected from the MCD64A1 product if (*i*) the uncertainty in day-of-burn for that pixel was 1 (the lowest) and (*ii*) was not isolated, that is, had at least one burned neighbouring pixel. The latter criterion was used because isolated burned area pixels often corresponded to small fires caused by human activities such as harvest stubble burning or hazard reduction burns. This selection resulted in a total of 295,151 fire occurrences in grassland; 1,055,006 for shrubland, and 1,036,277 for forest.

Unburned pixels were selected from cells surrounding the burned pixels using the semi-variogram geostatistical technique (Jurdao et al., 2012). A semi-variogram, $r(h)$ is used to measure the degree of dissimilarity between observations as a function of the distance between them and can be expressed as:

$$r(h) = \frac{1}{2N}\sum_{i=1}^{N}[Z(x_i) - Z(x_i + h)]^2 \quad (6)$$

where $Z(x_i)$ and $Z(x_i + h)$ are the FMC values of the pixels at distance x_i and $x_i + h$, and N is the total number of pixels that correspond to distance h.

Typically, the variance expressed in the semi-variogram is low between the burned pixel and nearby unburned pixels and increases with distance up to some threshold distance (known as the 'range'). Beyond this point, pixels can be considered uncorrelated with the burned pixel, and the variance achieves a stable maximum value (known as 'sill')

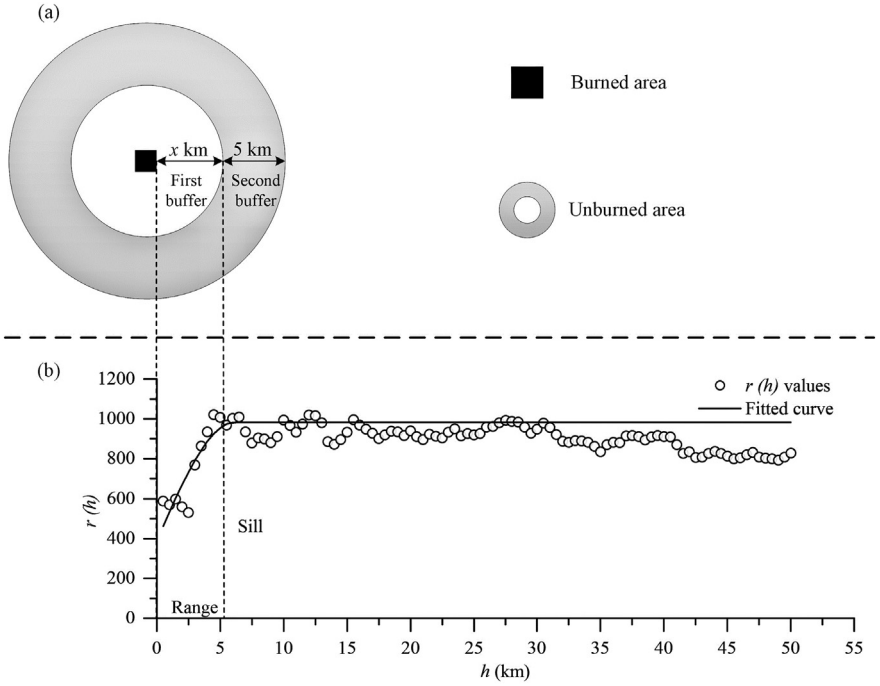

Fig. 3. (a) Diagram illustrating how the unburned pixels were selected and (b) example of the empirical semi-variogram and fitted model for FMC data on the 1/1/2003 (h30v12) illustrating the concepts of range and sill.

(Fig. 3). The range and sill were determined by fitting a spherical model (Jian et al., 1996) to the semi-variogram ($r(h)$) using the MATrix LABoratory (MATLAB) programming language. The first buffer around each burned pixel was established at the sill range distance, to avoid selecting non-fire pixels contaminated by actual burns (Fig. 3). A second buffer was placed at 5 km to delimit the unburned area. Unburned pixels further than 5 km from the first buffer were not included in the analysis to avoid including pixels with vegetation very different from that at the burn as much as possible,. All pixels included in the second buffer that were classified as the same vegetation type as the burned pixel and that were not affected by fire were included in the corresponding unburned pixel sample. The average of their corresponding FMC values was used to fit the logistic model. Once the burned and unburned pixels and the independent variables were selected, the coefficients of Eq. 4 were fitted using 20% of the total number of paired burned-unburned FMC values and the maximum likelihood estimation statistical method.

3.3. Live fuel moisture content and flammability evaluation

The coefficient of determination (R^2) and the Root Mean Squared Error (RMSE) were used to assess the FMC estimates generated in this study in comparison to field FMC measurements. These results were also compared to two empirical equations developed in previous studies for south-eastern Australia's shrubland (Caccamo et al., 2012) and forests (Nolan et al., 2016) for the same field dataset (Eqs. 7 and 8, respectively).

$$FMC = [85.93 + (NDII6_{max-min} \times 25.21) + (VARI_{max-min} \times 15.90)] \quad (7)$$

$$FMC = 52.51\, e^{1.36\, VARI_{max-min}} \quad (8)$$

where $NDII6_{max\text{-}min}$ and $VARI_{max\text{-}min}$ indicate the relative variation of NDII and VARI (the Visible Atmospheric Resistant Index, Eq. 9) (Gitelson et al., 2002) scaled between its maximum and minimum values over a period (2000–2016).

$$VARI = \frac{\rho_4 - \rho_1}{\rho_4 + \rho_1 - \rho_3} \quad (9)$$

where ρ_x is reflectance in MODIS band x.

The "Area Under the Curve" (AUC) calculated from the Receiver Operating Characteristic (ROC) plot method was calculated interpreted as a measure of the performance of the logistic flammability index for the training sample. The ROC is a graphical plot that illustrates the performance of a binary classifier system as its discrimination threshold is varied (Fielding and Bell, 1997). Given that the number of fire and non-fire events was equal in the training sample, an AUC value of 0.5 can be interpreted as equivalent to the toss of a coin, whereas a value of 1 would be a perfect prediction.

In addition, we analysed the temporal dynamics of average FMC values and corresponding flammability for the total burned extent before and after three big fire events in Australia. The objective of this temporal analysis was to corroborate the occurrence of higher fire risk conditions (i.e. lower FMC and greater flammability) during days preceding the fire events. The selected fire events were (*i*) the Canberra region fires that ignited on the 8th January 2003 and burned for around two weeks with the greatest area burning on the 17th and 18th of January 2003; (*ii*) widespread fire activity on 7th February 2009 in South-Eastern Australia, colloquially known as 'Black Saturday'and (iii) Linksview Road Fire, New South Wales (also called the Springwood Fire or Winmalee fire) that started on the 16th October 2013.

4. Results

4.1. Evaluation of fuel moisture content estimates

The median of the corresponding FMC values from the 40 to 1195 most similar spectra in the LUT achieved the most accurate FMC retrievals (Fig. 4). RMSE reached a minimum value (33%) when selecting 875 to 1995 spectra, but the R^2 between FMC observations and estimations was between 0.53 and 0.54 and not significant ($p = 0.08$). The 40 most similar spectra were preferred since they produced the highest R^2 of 0.57 ($p < 0.01$) and a modest RMSE increase (33% to 40%) with respect the use of 875 to 1995 spectra.

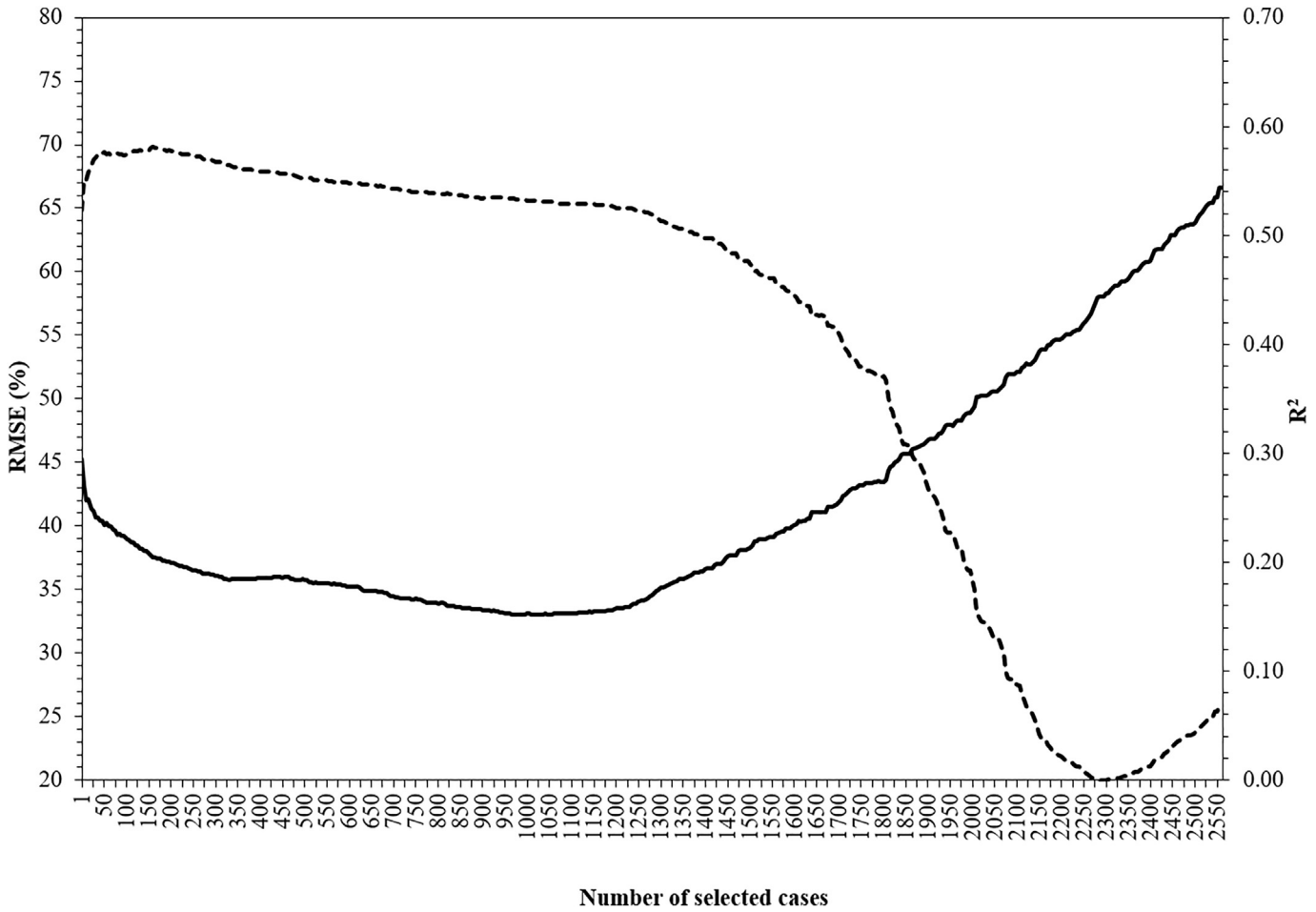

Fig. 4. RMSE (continuous line) and R^2 (dotted line) values between observed and estimated FMC as a function of the number of selected spectra in the LUT.

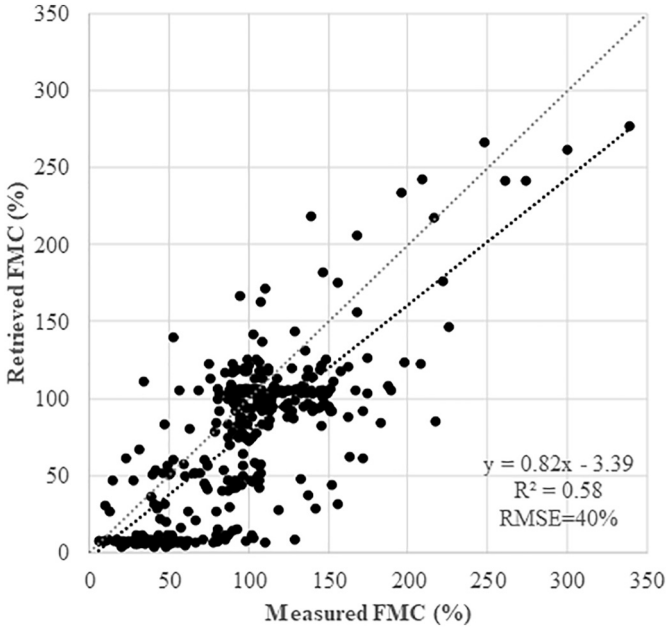

Fig. 5. Retrieved versus field-measured FMC (%) at all validation sites with its regression line (black dotted line) and the 1:1 regression line (grey dotted line).

Overall, the algorithm explained 58% of the variance in measured FMC across all sites and land cover classes with an RMSE of 40% (n = 360). The slope (0.82, $p < 0.001$) and offset (−3.39, p = 0.398) of the linear regression between measured and retrieved FMC (Fig. 5) suggest no significant bias in the estimates as well.

The standard deviation computed from the 40 FMC values may be considered a measure of uncertainty in the model inversion (ε_{FMC}) and therefore was expected to be correlated with the difference between the retrieved and measured FMCs. However, such a correlation was not found (Fig. 6). Instead, we did find a significant ($p < 0.001$) correlation between ε_{FMC} and both field-measured and retrieved FMC, suggesting that the inversion uncertainty is greater when FMC is higher (Fig. 6).

Considering individual land cover classes, the inversion model reproduced the patterns of low and high grassland FMC (R^2 = 0.60) but not those of shrubland (R^2 = 0.03) and forest (R^2 = 0.17). However, in absolute terms, the algorithm produced the best FMC estimates for shrubland (RMSE = 14%), followed by forest (RMSE = 32%) and grassland (RMSE = 49%). In other words, there was not much variance in the measured FMC for shrubland and forest.

There is large variability in the performance of the model for individual sites (Table 3). Momentarily only considering sites with 12 or more observations, RMSE varied between 12% (site 18) and 61% (site 4,), and R^2 values ranged between 0.27 (site 1) and 0.96 at site 4.

Lower RMSE between observed and retrieved FMC for grasslands was obtained when using our algorithm, compared to either of the empirical models developed by Caccamo et al. (2012) or Nolan et al. (2016) (hereafter referred as C2012 and N2016). Additionally, the retrievals tracked seasonal changes in grassland FMC better, with R^2 = 0.60 versus 0.22 for C2012 and 0.14 for N2016 (Table 3). The retrieval method performed similar to C2012 in reproducing absolute values of shrublands FMC (RMSE of 14% and 12% for this study and

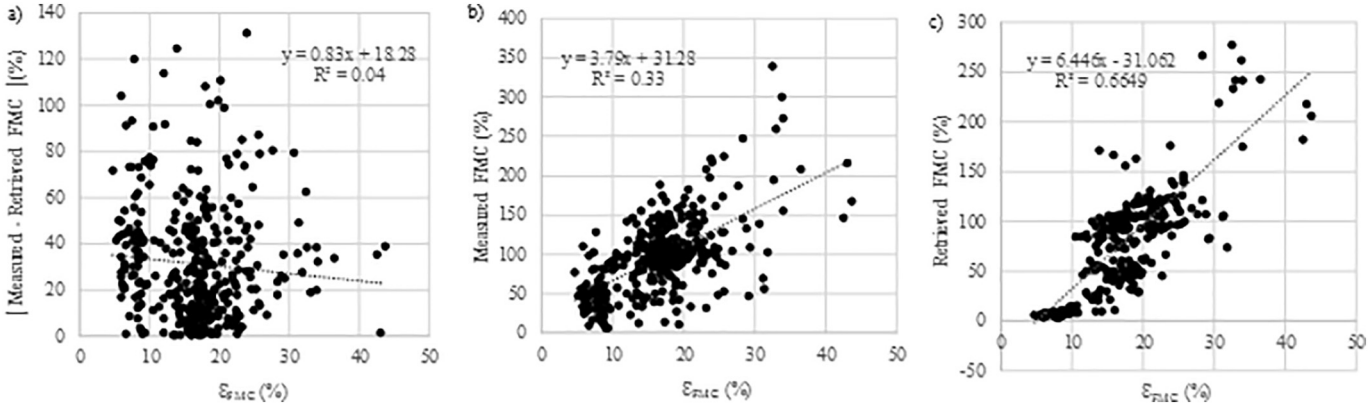

Fig. 6. Uncertainty in the model estimate (ε_{FMC}, computed as the standard deviation of the 40 FMC values selected from the LUT) versus (a) the deviation of the retrieved from the measured FMC (residual) (b) the measured FMC (%) and (c) the retrieved FMC (%).

Table 3
Relation between measured and retrieved FMC. The performance of the empirical models of Caccamo et al. (2012) (C2012) and Nolan et al. (2016) (N2016) empirical models for the same observations are included for comparison. R^2, the coefficient of determination; RMSE, root mean squared error; n, the number of samples; n.s, not significant correlation. * and + Indicate sites used for the calibration of N2016's empirical model and C2012, respectively. (Please note than the C2012 used a 70% and 30% random sample of the measurements taken in those sites for calibration and validation respectively).

Land cover class	ID	This study		C2012		N2016		n
		r^2	RMSE	r^2	RMSE	r^2	RMSE	
Grassland	1	0.27	60	0.58	51	0.47	40	37
	2	0.81	40	0.84	57	0.84	54	33
	3	0.70	61	0.79	78	0.69	76	33
	4	0.96	55	0.96	83	0.98	98	4
	5	n.s.	40	n.s.	38	n.s.	16	5
	6	n.s.	54	0.20	22	n.s.	34	5
	7	0.92	39	n.s.	61	0.89	49	7
	8	0.79	30	0.81	50	0.79	62	7
	9	n.s.	45	0.70	43	0.90	33	12
	10	0.83	27	0.82	61	0.70	60	9
	11	n.s.	51	n.s.	49	n.s.	31	4
	12	0.91	28	0.85	51	0.73	33	9
	13	n.s.	56	n.s.	55	n.s.	59	5
	14	0.67	26	n.s.	70	0.16	71	10
	All	0.60	49	0.22	59	0.14	55	180
Shrubland	15+	n.s.	14	0.62	13	0.51	33	15
	16+	0.40	15	0.80	13	0.54	18	13
	17+	n.s.	12	0.69	10	0.33	34	15
	All	n.s.	14	0.64	12	0.44	30	43
Forest	18+	n.s.	31	0.66	4	0.58	19	12
	19+	n.s.	19	n.s.	8	n.s.	17	12
	20+	n.s.	13	0.47	7	0.70	20	11
	21*	0.36	44	0.53	27	0.59	23	19
	22*	n.s.	23	n.s.	20	n.s.	34	10
	23	0.61	53	n.s.	55	n.s.	56	8
	24	n.s.	20	n.s.	6	n.s.	16	5
	25	n.s.	6	n.s.	7	n.s.	6	4
	26	n.s.	9	n.s.	7	n.s.	6	4
	27	n.s.	11	n.s.	8	n.s.	18	5
	28	n.s.	16	n.s.	9	n.s.	22	3
	29	n.s.	63	n.s.	69	n.s.	75	3
	30*	n.s.	10	0.92	7	0.91	10	4
	31	n.s.	34	0.28	23	0.28	18	19
	32	n.s.	36	0.58	28	0.50	12	18
	All	0.17	32	0.21	25	0.38	26	137
ALL	ALL	0.58	40	0.23	45	0.20	44	360

C2012, respectively) but better than N2016 (RMSE = 30%) (Table 3). However, both C2012 and N2016 better reproduced the patterns of shrub moisture contents (R^2 of 0.64 and 0.44, respectively) than our estimates (R^2 = 0.03). Finally, our method produced slightly poorer results (R^2 = 0.17 and RMSE = 32%) than C2012 (R^2 = 0.21 and RMSE = 25%) and N2016 (R^2 = 0.38 and RMSE = 26%) in estimating forest FMC.

4.2. Flammability Index

5000 samples of burned and unburned pixels pairs were randomly selected from the total number of fire events over the period in each grassland (295,151 events), shrubland (1,055,006) and forest (1,036,277) to test the significance of FMC differences and to select candidate predictor variables. Significant differences ($p < 0.05$) between burned and corresponding unburned pixels were found for FMC_{t-1}, FMC_{t-2}, FMC_D and FMC_A. Therefore, the logistic equation selected all four of them as predictor variables to fit the model. However, correlation testing showed that FMC_{t-2} was strongly correlated to FMC_{t-1} ($p < 0.05$) for the three land cover classes (Table 4) and therefore it was not considered in further analysis.

Three separate logistic regression models for flammability were fitted for grassland ($FI_{Grassland}$, Eq. 9), shrubland ($FI_{Shrubland}$, Eq. 10) and forest (FI_{Forest}, Eq. 11) obtaining an AUC from the ROC curves of 0.70, 0.78 and 0.71, respectively (Fig. 7):

$$FI_{Grassland} = 0.18 - 0.01*FMC_{t-1} + 0.02*FMC_D - 0.02*FMC_A \quad (9)$$

$$FI_{Shrubland} = 5.66 - 0.09*FMC_{t-1} + 0.005*FMC_D - 0.28*FMC_A \quad (10)$$

$$FI_{Forest} = 1.51 - 0.03*FMC_{t-1} + 0.02*FMC_D - 0.02*FMC_A \quad (11)$$

4.3. Multi-temporal dataset of FMC and flammability for Australia

A result of this study is a multi-temporal FMC and flammability

Table 4
Pearson's correlation matrix of the four candidate independent variables for grassland, shrubland and forest. The bold style indicates a high Pearson's coefficient ($p < 0.05$).

Land cover class	Pearson correlation	FMC_{t-1}	FMC_{t-2}	FMC_D	FMC_A
Grassland	FMC_{t-1}		**0.97**	0.11	0.50
	FMC_{t-2}	**0.97**		0.36	0.46
	FMC_D	0.11	0.36		0.03
	FMC_A	0.50	0.46	0.03	
Shrubland	FMC_{t-1}		0.90	−0.07	0.18
	FMC_{t-2}	**0.90**		0.37	0.11
	FMC_D	−0.07	0.37		−0.14
	FMC_A	0.18	0.11	−0.14	
Forest	FMC_{t-1}		**0.89**	−0.17	0.09
	FMC_{t-2}	**0.89**		0.30	0.06
	FD	−0.17	0.30		−0.05
	FMC_A	0.09	0.06	−0.05	

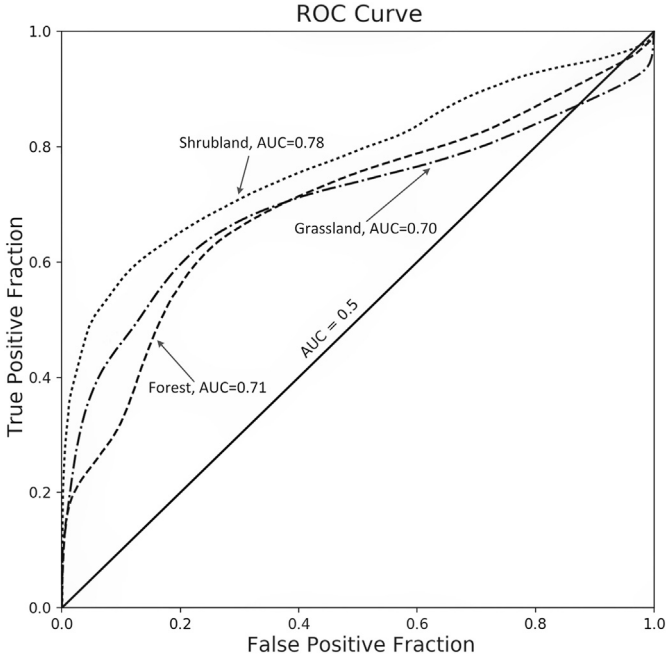

Fig. 7. ROC curve of logistic regression equations adjusted for grassland, shrubland and forest.

dataset at 8-day resolution for the period 2001 to 2017 over Australia. The dataset can be accessed via http://dapds00.nci.org.au/thredds/catalog/ub8/au/FMC/catalog.html. An example of FMC for 2015 is shown in Fig. 8. In January 2015, there were low FMC values in most of the temperate zones of Australia. FMC in these areas gradually increased until reaching their maximum at the end of winter or beginning of spring (e.g. August/September). Afterwards, FMC started to decrease until the end of the summer when values reach their minimum. In the tropical regions in the north of the country, the tendency was the opposite: higher values were observed during the northern wet season (Dec-March) and lower during the dry season (April–October). FMC values were consistently low in the desert zones.

4.4. Temporal FMC and FI dynamics before and after fire events

The average FMC decreased, and FI increased for the total burned extent for the different studied land cover classes in the months before the Canberra region fires that culminated on the 18 January 2003 (Fig. 9a). The major vegetation type burned during these fires was forest (82%), followed by grassland (18%) with negligible shrubland burned (0.1%). The average FMC for the total burned extent of a certain land cover class decreased from a monthly average of 132% and 91% in September to 27% and 79% in December for grasslandand and forest, respectively. Those changes in FMC involved an increase of 0.1 in the FI of grasslands (0.5 to 0.6) and forest (0.3 to 0.4).

The NSW fires also mainly affected forested areas (98%) followed by grassland (2%). The average grassland FMC within the burned extent first increased in winter from 202% (average of June) to 263% (average of July) and then decreased to 256% and 232% in August and September, respectively (Fig. 9b). The FI decreased from 0.50 to 0.42 then increased to 0.48 and 0.50. The forest FMC remained high (around 100%) over the months prior the fires, resulting in low and practically unchanged FI (Fig. 9b).

During the months prior the SE Australia 2009 fires, the grassland FMC decreased from 201% (October 2008) to 67% (January 2009) which resulted in an FI increase from 0.4 to 0.5 (Fig. 9c). There were only slight changes in forest FMC and FI with FMC values decreasing from 110% to 100%, and FI increasing from 0.2 to 0.3.

5. Discussion

The FMC estimation from RTM and its implementation to obtain flammability through logistic regression provides the first well-grounded model to predict fires one week before they occur across Australia.

There was a statistically significant ($p < 0.01$) agreement between retrieved and measured FMC at the 32 field sites used to evaluate the inverse RTM method. The RMSE of FMC estimates for grasslands (49%) and forest (32%) were greater than those for shrublands (14%). However, grassland showed higher FMC variability over time including FMC < 30% that are typical of dead fuels. Part of this variation was correctly detected in the retrievals, and as a consequence, the temporal correlation achieved was strongest for grassland ($R^2 = 0.6$).

The RMSE and R^2 in Table 3 are within the range reported by Yebra et al. (2013) for ten studies that performed an independent validation of FMC estimates obtained using different sensors and calibrated in various countries. The RMSE reported in those studies ranged between 25 and 61% for grasslands (Chuvieco et al., 2004b; García et al., 2008; Yebra et al., 2008), ≈30% for forest (Jurdao et al., 2013b; Yebra and Chuvieco, 2009a) and 8–20% for shrublands (Caccamo et al., 2012; García et al., 2008; Yebra and Chuvieco, 2009b). The inversion algorithm developed here predicted higher uncertainty in retrieving high FMC values. From a fire management perspective, higher uncertainty in higher FMC is likely to be less problematic than high uncertainty in low values, as high FMC values will normally be associated with lower rates of fire spread (Rossa et al., 2016).

The algorithm presented here was more accurate in retrieving FMC for grassland than the two other models developed for Australia. C2012 and N2016 are both empirical models, and are not calibrated for grasslands. The C2012 model better reproduced the seasonal variation in shrubland FMC ($R^2 = 0.64$). This was to be expected, as Caccamo et al. (2012) selected a 70% random data sample for calibration. They used sites also processed here: shrublands sites 15, 16 and 17, as well as forest sites 18, 19 and 20 (see Table 1). Conversely, C2012 did not perform so well at some of the forest plots excluded from calibration (e.g. sites 22, 23 and 29). These findings confirm previous evidence that empirical models have limited general applicability and should be re-calibrated when applied in different conditions (Nolan et al., 2016). Sites 21, 22 and 30 were used for calibrating N2016, whereas sites 23 to 29 were used for validation. Even so, their method produced the best estimates only for one of those sites (26). Nolan et al. (2016) adjusted the empirical equations in N2016 using reflectance data from the MOD09A1 (collection 5) product. Here we processed reflectance from MCD43A4 (collection 5), which suggests that Nolan et al. (2016) equations might be sensor-dependent. The sensor dependence of empirical models may also explain the slightly poorer performance of the C2012 model found here when compared to the results presented in Caccamo et al. (2012) ($R^2 = 0.687$ and RMSE = 7.98%, $n = 45$).

Good knowledge of the retrieval errors and uncertainties is critically important in assessing fire risk. The results presented here confirm the hypothesis that the LUTs developed for Spain can be used to retrieve FMC in Australia if MODIS landcover information is used to constrain the inversion. However, misclassifications are important since they will propagate to errors in the computation of FMC given an incorrect LUT will be selected to constrain the LUT inversion. The overall accuracy (percentage of the total number of correctly classified pixels divided over the total number of test pixels) for the classification map was 76% based on the sampling sites ($n = 363$). The main confusions occurred for shrublands pixels that were included into the forest class (45 times) and grasslands assessed as shrublands (43 times). The former misclassifications are probably more problematic as grasslands and forest have more contrasting structural and spectral properties than grasslands and shrublands. The grasslands and shrublands spectra were simulated using PROSPECT+SAILH turbid medium RTM while the spectra of forest were simulated using a geometrical RTM (GeoSAIL)

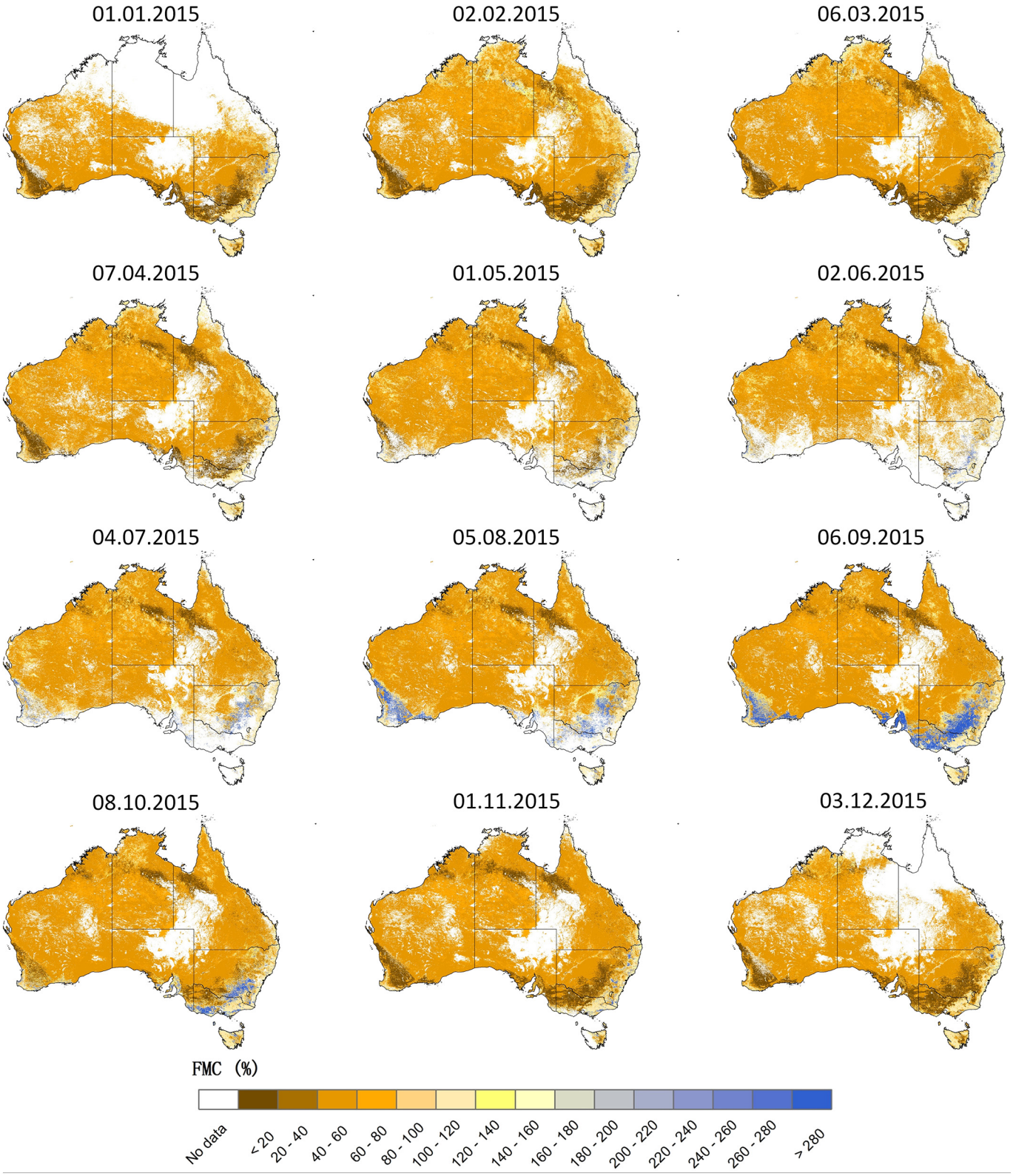

Fig. 8. Multi-temporal FMC change in Australia for 2015. Areas that are masked by white are non-assessed land cover classes, e.g. urban areas and water bodies, and missing data, e.g. due to clouds cover.

that accounts for the effects of shadows cast by the canopy.

For validation we relied on existing and new FMC data that were collected and processed following sometimes very different protocols, which introduces further uncertainties. For example, different drying temperatures and times were used. Matthews (2010) demonstrated that oven-drying does not measure true FMC, and the gravimetric FMC final values are strongly dependent on (oven) drying temperature and the ambient air humidity the sample may have been exposed to before weighing.

Another important challenge is to obtain representative and

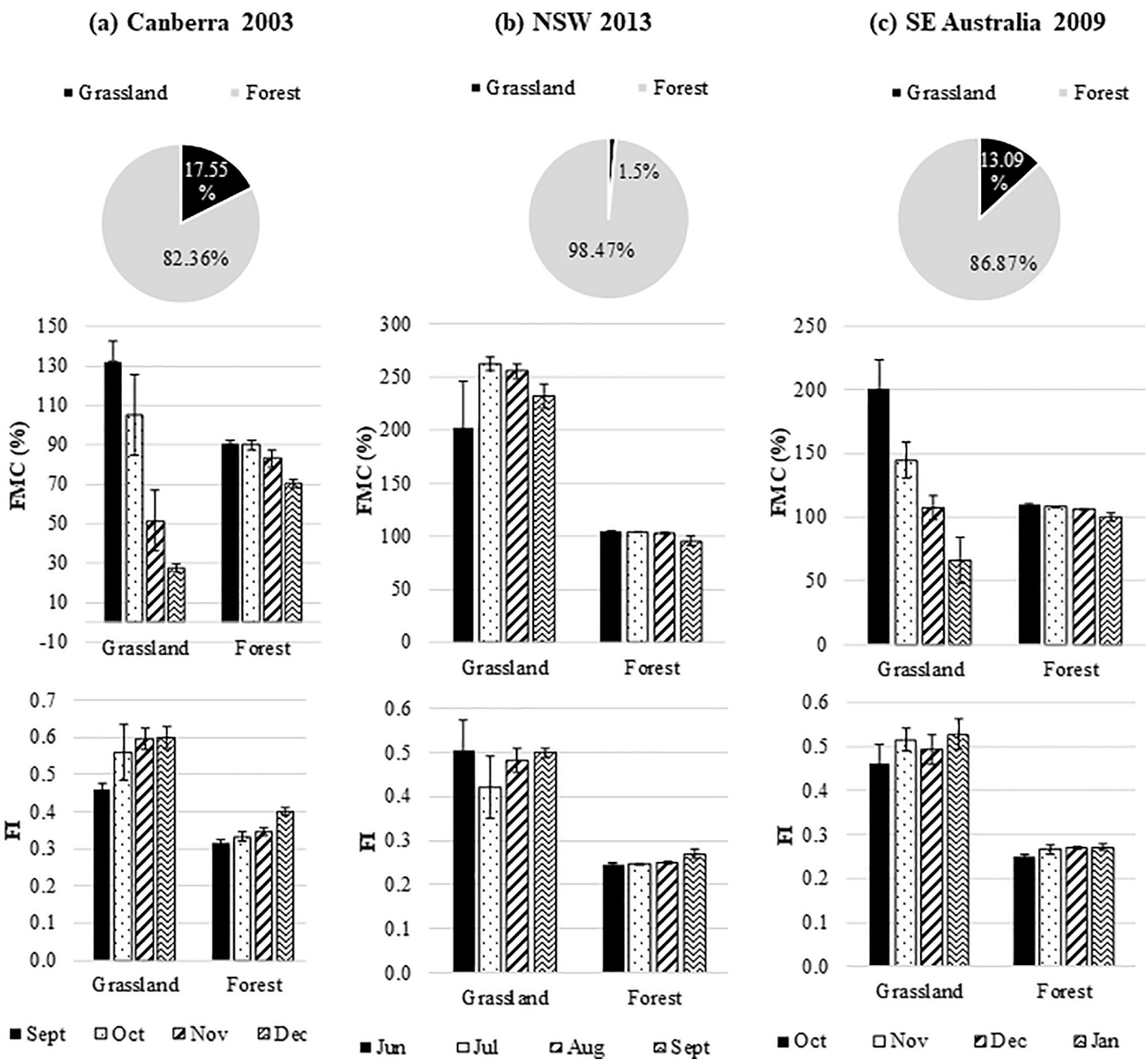

Fig. 9. Percentage of total burned area per land cover type (pie charts) and estimated temporal FMC and FI dynamics for the months right before the bushfire events occurred (bar charts). The FMC and FI values are averaged for each month, land cover class and burned extent. Error bars represent one standard deviation of the FMC or FI for each month, land cover and burned extent.

accurate field measurements for validation. This is especially true in multi-layer forest. When this forest presents a dense and closed canopy, the satellite sensor will only observe the top of the canopy, and therefore, only FMC from the canopy should be used for validation. Conversely, in more open forest, the understory layer may also be exposed to the sensor. In this situation, a simple average of the FMC of both top canopy and understory layers, or an average of each layer weighted by the satellite-exposed cover fraction would be better suited to evaluate FMC retrievals. Here we used the simple average of FMC measured for all layers (where separately reported) as a measurement of plot level FMC, without consideration of the openness of the forest or the visible fraction of each layer. Future research could investigate whether a measure of forest cover might improve the representativeness of the plot level field measured FMC in satellite retrieval validation. From a practical perspective, it is not necessarily clear what the preferred approach would be to characterise the FMC of different vegetation strata in a single value. Likely, it would depend on whether the resulting values are to be used to predict the risk of ignition, rate of spread, or difficulty of suppression.

A final factor causing uncertainty in validation is that the reflectance data for each pixel were derived from a 16-day composite. We minimized the number of days between field and satellite observations by matching field observations to the MODIS composite that contained the observations of the 8 days in the middle. However, potential changing weather conditions between field measurements and composite day may have increased the uncertainties in the retrievals.

Better accuracy and prediction of temporal patterns for forests and shrublands is very desirable to further improve fire risk estimation and use by practitioners. The broad-leaf PROSPECT optical properties model used here was mainly derived from European vegetation types. Australian forest species have different radiative transfer properties, mainly caused by the wax coating and anthocyanins in the leaves (Barry

et al., 2009). Further research requires advancement towards physically-based satellite FMC monitoring methods through the development of a suite of radiative transfer models adapted for Australian temperate sclerophyll forest. The recently developed PROSPECT-D adds the modelling of the carotenoid and anthocyanin content (Féret et al., 2017), but does not account for the presence of wax at the leaf surface in Eucalyptus to compute the reflectance. (Féret et al., 2017) Prescribing LAI to a known value can also improve RTM inversion to retrieve FMC (Yebra et al., 2008; Zarco-Tejada et al., 2003). Instead, errors in LAI products can also introduce new errors in the RTM inversion (Jurdao et al., 2013b). Therefore, the merit of including these information needs further testing.

Three logistic regression models were developed separately for grassland, shrubland and forest to relate fire occurrence to the observed FMC in the 8-day period before the fire. The advantage of these models is that they offer the possibility of predicting fire risk at least a week ahead. Despite the inaccuracies detected in the FMC estimates, we obtained an AUC from the ROC for grassland (0.70) and shrubland (0.78) that was higher than obtained by Jurdao et al. (2012) over Spain (0.62 and 0.67 for grassland and shrubland, respectively; forests were not considered in their analysis). Jurdao et al. (2012) derived fire occurrence from a NOAA-AVHRR based empirical FMC product (García et al., 2008) and fire occurrence from the standard MODIS Thermal Anomalies product (MOD14), both for 2001–2007. Here we used a MODIS- and physically-based FMC product, which has higher spatial resolution, and the MCD64A1 burned area product, which is the most accurate global BA product for a longer time series (2001–2016). These may explain the better performance of the models developed here.

The average FMC and FI for the total burned extent for the different land cover classes suggested the occurrence of higher fire risk conditions (e.g. lower FMC and greater flammability) during the days preceding the case studies examined here. FMC decreased, and FI increased in the months before the 2003 Canberra fires. The significantly drier than normal conditions in the months before the fires (Taylor and Webb, 2005) led to low FMC for grassland (27%) and forest (79%), and as a consequence, the FI was relatively high. September 2013 was the warmest September on record in the Greater Blue Mountain areas affected by the NSW fires and experienced below-average rainfall (BoM, 2013). Although FMC values averaged over the subsequently burned grassland areas were still high in September 2013 (> 200%) they were still below average and resulted in a high departure from the average FMC value for the time series (2001–2016). As a result, the FI of grassland areas was elevated. Finally, the cumulative effect of successive years of below-average rainfall before 2009 affected groundwater levels and soil moisture throughout south-east Australia (van Dijk et al., 2013) as well as increased dryness of live vegetation and coarse woody debris (Gill and Moore, 1990). On 7 February 2009 values of the Keetch-Byram Drought Index (Keetch and Byram, 1968) for some areas in the Yarra Valley were up to 50% higher than the normal level expected at that time of the year (40 years average) (Cruz et al., 2012). Those hot and dry conditions may explain the lower FMC and higher FI in January comparing to October, especially for grasslands.

Although the average FMC and FI for the total burned extent for the different land cover classes suggested the occurrence of higher fire risk conditions (e.g. lower FMC and greater flammability) during the previous days of the different fire events examined here, the long-term objective is to integrate FMC with other key fuel structural properties and fire weather into fire propagation models, to derive more reliable estimates of flammability and rate of spread for local conditions. Quantitative integration of these additional factors can be achieved by including them in the same additive logistic models applied here. Such an approach provides a complete assessment of risk conditions, which might produce better results than current methods that are focused on meteorological variables.

The availability of frequent, rapid turn-around and pre-processed imagery from the European Sentinel-2 satellites has created an opportunity to develop real-time monitoring capability at much higher spatial resolution (10–60 m). This increase in spatial resolution would likely strongly increase our understanding of forest flammability as well as support a wider range of fire management activities.

6. Conclusion

We presented the first Australia-wide product of FMC and associate flammability based on MODIS imagery and radiative transfer model inversion. The FMC model was first developed for Spain and here applied to Australia without further modification. A total of 360 FMC measurements at 32 grassland, shrubland and forested sites were used to assess the accuracy of the FMC estimates. We consider our results encouraging, given (1) the method was calibrated for Spanish vegetation types and applied to a continent with vastly different climate conditions and ecosystems, and (2) the uncertainty of some of the field measurements, especially for forests. Nevertheless, a reduction of estimation error, particularly at low FMC levels, is very desirable to further improve fire risk estimation and use by practitioners.

FMC was converted into a flammability index estimates using logistic regression models, offering the possibility to predict fires one week before the beginning of the event. Future work will focus on integrating FMC with other key fuel structural properties and fire weather into fire propagation models, to derive more reliable estimates of flammability and rate of spread for local conditions.

Acknowledgements

This work was funded from the Bushfire and Natural Hazards CRC through the Mapping Bushfire Hazard and Impacts project. An ANU Centre for European Studies Visiting Fellowship and an UC-Davis Professional Development Award funded David Riaño to participate in this study. We thank our lead end user Dr. Adam Leavesley and his colleagues from ACT Parks and Conservation Service, for their continued enthusiastic engagement, valuable feedback and support for the fieldwork. Fieldwork support by Ms. Lauren de Waal and Caroline Luiz is also valued. We also thank Glenn Newnham, Gabriele Caccamo, Ross Bradstock, Matthias Boer and Rachael Nolan for providing field FMC measurements for validation sites used in this study. Hwan-Jin Yoon guidance in the statistical analysis is also acknowledged.

References

Al-Moustafa, T., Armitage, R.P., Danson, F.M., 2012. Mapping fuel moisture content in upland vegetation using airborne hyperspectral imagery. Remote Sens. Environ. 127, 74–83.
Anderson, H.E., 1970. Forest fuel ignitibility. Fire. Technol 6, 312–319.
Barry, K.M., Newnham, G.J., Stone, C., 2009. Estimation of chlorophyll content in Eucalyptus globulus foliage with the leaf reflectance model PROSPECT. Agric. For. Meteorol. 149, 1209–1213.
BoM, 2013. Monthly Weather Review Australia. September 2013. Publishing Unit, Bureau of Meteorology, GPO Box 1289, Melbourne VIC 3001.
Bowyer, P., Danson, F.M., 2004. Sensitivity of spectral reflectance to variation in live fuel moisture content at leaf and canopy level. Remote Sens. Environ. 92, 297–308.
Caccamo, G., Chisholm, L.A., Bradstock, R.A., Puotinen, M.L., Pippen, B.G., 2012. Monitoring live fuel moisture content of heathland, shrubland and sclerophyll forest in South-Eastern Australia using MODIS data. Int. J. Wildland Fire 21, 257–269.
Casas, A., Riaño, D., Ustin, S.L., Dennison, P., Salas, J., 2014. Estimation of water-related biochemical and biophysical vegetation properties using multitemporal airborne hyperspectral data and its comparison to MODIS spectral response. Remote Sens. Environ. 148, 28–41.
Chuvieco, E., Aguado, I., Dimitrakopoulos, A.P., 2004a. Conversion of fuel moisture content values to ignition potential for integrated fire danger assessment. Can. J. For. Res. 34, 2284–2293.
Chuvieco, E., Cocero, D., Riaño, D., Martin, P., Martínez-Vega, J., de la Riva, J., Pérez, F., 2004b. Combining NDVI and surface temperature for the estimation of live fuel moisture content in forest fire danger rating. Remote Sens. Environ. 92, 322–331.
Chuvieco, E., Gonzalez, I., Verdu, F., Aguado, I., Yebra, M., 2009a. Prediction of fire occurrence from live fuel moisture content measurements in a Mediterranean ecosystem. Int. J. Wildland Fire 18, 430–441.
Chuvieco, E., Wagtendonk, J., Riaño, D., Yebra, M., Ustin, S.L., 2009b. Estimation of Fuel Conditions for Fire Danger Assessment. Springer.

Chuvieco, E., Aguado, I., Jurdao, S., Pettinari, M.L., Yebra, M., Salas, J., Hantson, S., de la Riva, J., Ibarra, P., Rodrigues, M., Echeverria, M., Azqueta, D., Roman, M.V., Bastarrika, A., Martinez, S., Recondo, C., Zapico, E., Martinez-Vega, F.J., 2014. Integrating geospatial information into fire risk assessment. Int. J. Wildland Fire 23, 606–619.

Cruz, M.G., Sullivan, A.L., Gould, J.S., Sims, N.C., Bannister, A.J., Hollis, J.J., Hurley, R.J., 2012. Anatomy of a catastrophic wildfire: the black Saturday Kilmore east fire in Victoria, Australia. For. Ecol. Manag. 284, 269–285.

Dennison, P.E., Moritz, M.A., 2009. Critical live fuel moisture in chaparral ecosystems: a threshold for fire activity and its relationship to antecedent precipitation. Int. J. Wildland Fire 18, 1021–1027.

Féret, J.B., Gitelson, A.A., Noble, S.D., Jacquemoud, S., 2017. PROSPECT-D: towards modeling leaf optical properties through a complete lifecycle. Remote Sens. Environ. 193, 204–215.

Fielding, A.H., Bell, J.F., 1997. A review of methods for the assessment of prediction errors in conservation presence/absence models. Environ. Conserv. 24, 38–49.

Friedl, M.A., Sulla-Menashe, D., Tan, B., Schneider, A., Ramankutty, N., Sibley, A., Huang, X.M., 2010. MODIS collection 5 global land cover: algorithm refinements and characterization of new datasets. Remote Sens. Environ. 114, 168–182.

García, M., Chuvieco, E., Nieto, H., Aguado, I., 2008. Combining AVHRR and meteorological data for estimating live fuel moisture content. Remote Sens. Environ. 112, 3618–3627.

Giglio, L., Loboda, T., Roy, D.P., Quayle, B., Justice, C.O., 2009. An active-fire based burned area mapping algorithm for the MODIS sensor. Remote Sens. Environ. 113, 408–420.

Gill, A.M., Moore, P.H.R., 1990. Fire intensities in eucalyptus forests of Southeastern Australia. In: International Conference on Forest Fire Research, pp. B24:21–12 (Coimbra, Portugal).

Gitelson, A.A., Stark, R., Grits, U., Rundquist, D., Kaufman, Y., Derry, D., 2002. Vegetation and soil lines in visible spectral space: a concept and technique for remote estimation of vegetation fraction. Int. J. Remote Sens. 23, 2537–2562.

Hao, X.J., Qu, J.J., 2007. Retrieval of real-time live fuel moisture content using MODIS measurements. Remote Sens. Environ. 108, 130–137.

Hardisky, M.A., Klemas, V., Smart, R.M., 1983. The influence of soil-salinity, growth form, and leaf moisture on the spectral radiance of Spartina-Alterniflora canopies. Photogramm. Eng. Remote. Sens. 49, 77–83.

Huemmrich, K.F., 2001. The GeoSail model: a simple addition to the SAIL model to describe discontinuous canopy reflectance. Remote Sens. Environ. 75, 423–431.

Jacquemoud, S., Baret, F., 1990. Prospect - a model of Leaf Optical-properties spectra. Remote Sens. Environ. 34, 75–91.

Jian, X.D., Olea, R.A., Yu, Y.S., 1996. Semivariogram modeling by weighted least squares. Comput. Geosci. 22, 387–397.

Jurdao, S., Chuvieco, E., Arevalillo, J.M., 2012. Modelling fire ignition probability from satellite estimates of live fuel moisture content. Fire Ecol. 8, 77–97.

Jurdao, S., Yebra, M., Chuvieco, E., 2013a. Live fuel moisture content derived from remote sensing estimates in temperate shrublands and grasslands. In: Earthzine.

Jurdao, S., Yebra, M., Guerschman, J.P., Chuvieco, E., 2013b. Regional estimation of woodland moisture content by inverting radiative transfer models. Remote Sens. Environ. 132, 59–70.

Jurdao, S., Yebra, M., Oliva, P., Chuvieco, E., 2014. Laboratory measurements of plant drying: implications to estimate moisture content from radiative transfer models in two temperate species. Photogramm. Eng. Remote. Sens. 80, 451–459.

Keetch, J.J., Byram, G.M., 1968. A drought index for forest fire control. Southeast. In: Forest Exp. Sta., USDA Forest Service Res. Pap. SE-38, pp. 32.

Kruse, F.A., Lefkoff, A.B., Boardman, J.W., Heidebrecht, K.B., Shapiro, A.T., Barloon, P.J., Goetz, A.F.H., 1993. The spectral image-processing system (sips) - interactive visualization and analysis of imaging spectrometer data. Remote Sens. Environ. 44, 145–163.

Kuusk, A., 1991. The hot-spot effect in the leaf canopy. In: Igarss 91 - Remote Sensing: Global Monitoring for Earth Management. Vol 1–4. pp. 1555–1557.

Loveland, T.R., Belward, A.S., 1997. The IGBP-DIS global 1km land cover data set, DISCover: first results. Int. J. Remote Sens. 18, 3289–3295.

Lymburner, L., Tan, P., Mueller, N., Thackway, R., Thankappan, M., Islam, A., Lewis, A., Randall, L., Senarath, U., 2011. In: T.R.R. 2011/031 (Ed.), The National Dynamic Land Cover Dataset. Geoscience Australia, Canberra.

Matthews, S., 2010. Effect of drying temperature on fuel moisture content measurements. Int. J. Wildland Fire 19, 800–802.

Newnham, G.J., Verbesselt, J., Grant, I.F., Anderson, S.A.J., 2011. Relative greenness index for assessing curing of grassland fuel. Remote Sens. Environ. 115, 1456–1463.

Nolan, R.H., Boer, M.M., Resco de Dios, V., Caccamo, G., Bradstock, R.A., 2016. Large-scale, dynamic transformations in fuel moisture drive wildfire activity across south-eastern Australia. Geophys. Res. Lett. 43, 4229–4238.

Padilla, M., Stehman, S.V., Ramo, R., Corti, D., Hantson, S., Oliva, P., Alonso-Canas, I., Bradley, A.V., Tansey, K., Mota, B., Pereira, J.M., Chuvieco, E., 2015. Comparing the accuracies of remote sensing global burned area products using stratified random sampling and estimation. Remote Sens. Environ. 160, 114–121.

Peterson, S.H., Roberts, D.A., Dennison, P.E., 2008. Mapping live fuel moisture with MODIS data: a multiple regression approach. Remote Sens. Environ. 112, 4272–4284.

Rossa, C.G., Veloso, R., Fernandes, P.M., 2016. A laboratory-based quantification of the effect of live fuel moisture content on fire spread rate. Int. J. Wildland Fire 25, 569–573.

Roy, D.P., Wulder, M.A., Loveland, T.R., C.E., W., Allen, R.G., Anderson, M.C., Helder, D., Irons, J.R., Johnson, D.M., Kennedy, R., Scambos, T.A., Schaaf, C.B., Schott, J.R., Sheng, Y., Vermote, E.F., Belward, A.S., Bindschadler, R., Cohen, W.B., Gao, F., Hipple, J.D., Hostert, P., Huntington, J., Justice, C.O., Kilic, A., Kovalskyy, V., Lee, Z.P., Lymburner, L., Masek, J.G., McCorkel, J., Shuai, Y., Trezza, R., Vogelmann, J., Wynne, R.H., Zhu, Z., 2014. Landsat-8: science and product vision for terrestrial global change research. Remote Sens. Environ. 145, 154–172.

Stephens, S.L., Burrows, N., Buyantuyev, A., Gray, R.W., Keane, R.E., Kubian, R., Liu, S.R., Seijo, F., Shu, L.F., Tolhurst, K.G., van Wagtendonk, J.W., 2014. Temperate and boreal forest mega-fires: characteristics and challenges. Front. Ecol. Environ. 12, 115–122.

Strahler, A.H., Muller, J.P., Modis Sciences Team Members, 1999. MODIS BRDF Albedo Product: Algorithm Theoretical Basis Document Version 5.0. pp. 53.

Taylor, J., Webb, R., 2005. Meteorological aspects of the January 2003 south-eastern Australia bushfire outbreak. Aust. For. 68, 94–103.

van der Walt, S., Colbert, S.C., Varoquaux, G., 2011. The NumPy Array: a structure for efficient numerical computation. Comput. Sci. Eng. 13, 22–30.

van Dijk, A.I.J.M., Beck, H.E., Crosbie, R.S., de Jeu, R.A.M., Liu, Y.Y., Podger, G.M., Timbal, B., Viney, N.R., 2013. The millennium drought in Southeast Australia (2001–2009): natural and human causes and implications for water resources, ecosystems, economy, and society. Water Resour. Res. 49, 1040–1057.

Verhoef, W., 1984. Light-scattering by leaf layers with application to canopy reflectance modeling - the Sail model. Remote Sens. Environ. 16, 125–141.

Yebra, M., Chuvieco, E., 2009a. Generation of a species-specific look-up table for fuel moisture content assessment. IEEE J. Sel. Top. Appl. Earth Observ. Remote Sens. 2, 21–26.

Yebra, M., Chuvieco, E., 2009b. Linking ecological information and radiative transfer models to estimate fuel moisture content in the Mediterranean region of Spain: solving the ill-posed inverse problem. Remote Sens. Environ. 113, 2403–2411.

Yebra, M., Chuvieco, E., Riano, D., 2008. Estimation of live fuel moisture content from MODIS images for fire risk assessment. Agric. For. Meteorol. 148, 523–536.

Yebra, M., Dennison, P.E., Chuvieco, E., Riano, D., Zylstra, P., Hunt, E.R., Danson, F.M., Qi, Y., Jurdao, S., 2013. A global review of remote sensing of live fuel moisture content for fire danger assessm6ent: moving towards operational products. Remote Sens. Environ. 136, 455–468.

Youngentob, K.N., Zdenek, C., van Gorsel, E., 2016. A simple and effective method to collect leaves and seeds from tall trees. Methods Ecol. Evol. 7, 1119–1123.

Zarco-Tejada, P.J., Rueda, C.A., Ustin, S.L., 2003. Water content estimation in vegetation with MODIS reflectance data and model inversion methods. Remote Sens. Environ. 85, 109–124.